Anisotropic paramagnetism of Co-doped ZnO epitaxial films

A. Ney,* T. Kammermeier, K. Ollefs, S. Ye, and V. Ney
Fakultät für Physik and CeNIDE, Universität Duisburg-Essen, Lotharstrasse 1, D-47057 Duisburg, Germany

T. C. Kaspar and S. A. Chambers
Fundamental and Computational Sciences Directorate, Pacific Northwest National Laboratory, Richland, Washington 99352, USA

F. Wilhelm and A. Rogalev
European Synchrotron Radiation Facility (ESRF), 6 Rue Jules Horowitz, BP 220, 38043 Grenoble Cedex, France
(Received 10 September 2009; revised manuscript received 8 January 2010; published 17 February 2010)

We have measured the full temperature dependence of $M(H)$ curves for 5%, 10%, and 15% Co-doped ZnO epitaxial films with high crystalline perfection. Bulk magnetometry reveals pure paramagnetism with anisotropic $M(H)$ curves at low temperatures, whereas the x-ray magnetic circular dichroism measured at the Co K edge is isotropic. Electron paramagnetic resonance shows that the g factors are not significantly altered compared to Co^{2+} impurities in ZnO. The $M(H)$ measurements are compared to simulations using either an effective spin model with zero-field splitting D or Brillouin functions with an effective temperature ansatz. Whereas both models reproduce well the $H \perp c$ data, for $H \| c$ the effective spin model indicates that D is reduced by 75% compared to Co^{2+} impurities in ZnO. The dependence of the $M(H)$ curves and D on the Co concentration is discussed in terms of magnetic interactions between the Co dopant atoms.

DOI: 10.1103/PhysRevB.81.054420 PACS number(s): 75.50.Pp, 75.70.−i, 75.30.Hx

I. INTRODUCTION

Candidate dilute magnetic semiconductors based on oxide materials are widely studied systems. For Co-doped ZnO (Co:ZnO) early investigations were restricted to electron paramagnetic resonance (EPR) studies[1] or optical absorption measurements[2] in which Co^{2+} was present at the impurity level (10 ppm Co in Ref. 2) in ZnO single crystals. The renewed interest in this compound is stirred by experimental reports and theoretical predictions of room-temperature ferromagnetism in the concentration range of a few at. % Co in ZnO films. For the case of phase pure polycrystalline bulk Co:ZnO the absence of ferromagnetism has been demonstrated fairly early up to high Co concentrations and antiferromagnetic interactions between next-cation neighbor Co ions have been inferred from a Curie-Weiss analysis.[3,4] Nonetheless, the presence or absence of ferromagnetism in Co:ZnO remains controversial up to now, see, e.g., Ref. 5 for a recent overview. The controversy is caused by the fact that it is experimentally very challenging to rule out the formation of secondary Co-containing phases which can account for ferromagneticlike behavior. Metallic Co nanoclusters have recently been found in Co:ZnO by careful x-ray diffraction (XRD) analysis[6] and x-ray photoelectron spectroscopy depth profiling.[7] In recent studies, where phase separation is ruled out by detailed synchrotron methods, ferromagnetic order is found to be absent in high-quality epitaxial films of Co:ZnO.[5,8,9] Antiferromagnetic interaction between next-cation neighbor Co ions was inferred by a detailed analysis of superconducting quantum interference device (SQUID) magnetometry data accounting for the drop in expected magnetization with increasing Co content.[8,10] Moreover, the absence of ferromagnetic ordering is in agreement with recent *ab initio* simulations in the relevant Co concentration range.[11,12] On the other hand it was shown that Co:ZnO possesses a considerable single ion magnetic anisotropy with anisotropic $M(H)$ curves if the external magnetic field H is parallel or perpendicular to the c axis of the wurtzite lattice of ZnO.[13] However, such anisotropic $M(H)$ curves do not constitute a proof of ferromagnetism by themselves. They are merely a result of the spin-orbit (SO) interaction of a paramagnetic impurity in an anisotropic crystal field.

In this paper we show that for high Co concentrations in ZnO in the range of 5–15 % phase purity can inferred from x-ray absorption near-edge spectroscopy (XANES) and x-ray linear dichroism (XLD) recorded at the Co K edge. No indications of ferromagnetism are consistently found for three different samples fabricated with two different preparation techniques. Anisotropic $M(H)$ curves are observed over a range of temperatures by integral SQUID magnetometry. In contrast, element-specific x-ray magnetic circular dichroism (XMCD) spectra at the Co K edge are found to be isotropic. The anisotropic $M(H)$ curves and the associate temperature dependences can be satisfyingly modeled using the well-established effective spin model[1,2,13] comprising effective g factors ($g_\perp$ and $g_\|$) and a zero-field splitting $2D$. A comparison of EPR spectra of Co^{2+} impurities in ZnO with our epitaxial films demonstrates that the effective g factors remain essentially unchanged. However, the zero-field splitting ($2D$) for Co^{2+} impurities in bulk ZnO of 3.97 K is reduced at high Co concentrations to ~3 K for 5% and 10% Co and further to ~2 K for 15% of Co. Alternatively, the Brillouin function B_S can be used together with a simple effective temperature model to model the $M(H)$ curves. These findings will be discussed with respect to a statistical dopant distribution and an antiferromagnetic next-cation neighbor interaction.

II. EXPERIMENTAL DETAILS

Co:ZnO(0001) epitaxial films were deposited on polished 10 mm × 10 mm × 0.5 mm c plane single crystal

$Al_2O_3(0001)$ sapphire substrates from Crystec GmbH using either pulsed laser deposition (PLD) or reactive magnetron sputtering (RMS). The PLD-grown sample containing 10.8 at. % Co ions was 104 nm thick and was the basis of the study reported in Ref. 8. Co:ZnO films containing 5–15 % Co were grown in ultrahigh vacuum (UHV) by dc-RMS using metallic ZnCo targets of the desired composition. The film thickness ranged from 100 to 160 nm. One thick (~ 1 μm) 5% film was grown for EPR measurements to increase the magnetic signal for a given Co concentration. The base pressure of the UHV system was $\leq 1 \times 10^{-9}$ mbar. The working pressure in the chamber during film deposition was 4×10^{-3} mbar. The composition of the sputter gas ($Ar:O_2$) was controlled via separated mass flow controllers. It was found that $Ar:O_2$ ratios of 10:1 (10% and 15% Co) and 10:0.8 (5% Co) lead to structurally excellent paramagnetic Co:ZnO films. For all RMS growths, the substrate temperature was kept at 350 °C.

The XANES spectra were taken at the ID12 beamline of the ESRF in total fluorescence yield.[14] XLD spectra were measured at 300 K as the direct difference of XANES spectra recorded under 10° grazing incidence with two orthogonal linear polarizations. A quarter-wave plate was used to flip the linear polarization of the synchrotron light from vertical to horizontal, i.e., the E vector of the synchrotron light was either parallel or perpendicular to the c axis of the ZnO epitaxial film. The XMCD measurements were taken at 6.5 K as the direct difference of XANES spectra recorded with right and left circular polarized light for $H=6$ T under normal and grazing incidence (15°), respectively. To minimize artifacts, the direction of the external magnetic field was reversed as well.

The integral in-plane and out-of-plane magnetic measurements were performed in a temperature range from 2 to 300 K using a commercial SQUID magnetometer taking great care to minimize artifacts.[15] In particular, the edges of the substrate were thoroughly cleaned to avoid ferromagnetic contamination. In addition, all angular-dependent SQUID measurements were carried out on the same piece of sample inside the same SQUID sample holder (a clear drinking straw). The sample could be freely rotated inside the straw due to its size which was $\sim 4 \times 4$ mm^2. It is crucial that out-of-plane loops are measured first so that the indentations in the straw are identical for both measurements, cf. Ref. 15.

In addition, EPR spectra were recorded as a function of the polar angle Θ using X-band microwave frequencies (~ 9 GHz) at 5 K using a resonator-based spectrometer together with a liquid He flow cryostat and an electromagnet providing $H = \pm 1.2$ T. The integral structural properties were routinely characterized by XRD which reveals for all studied samples a c plane orientation for the ZnO films and no indication of additional crystallographic phases within the detection limit of XRD, i.e., ruling out Co crystallites above $\sim 2-4$ nm diameter, cf. Ref. 6.

III. EXPERIMENTAL RESULTS AND MODELING

In this section we give a comprehensive magnetic characterization of the Co:ZnO epitaxial films using XMCD, SQUID, and EPR. All measurements were performed by applying the external magnetic field H either parallel or perpendicular to the c axis of the ZnO. In addition, structural characterization was done by means of element-specific XLD which is highly sensitive to the local structural properties and the chemical state of the probed element.[8,9]

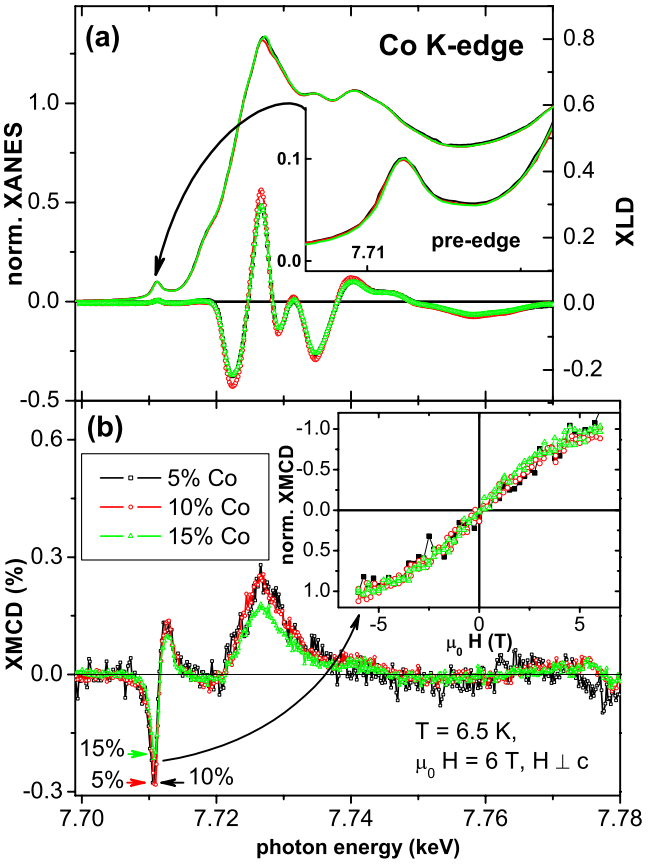

FIG. 1. (Color online) XANES, XLD, and XMCD spectra recorded at the Co K edge for three RMS-grown Co:ZnO samples with different Co concentrations. (a) The XLD signal for the three concentrations is of comparable size. The inset shows the pre-edge feature demonstrating the absence of measurable amounts of elemental Co^0. (b) The maximum size of the XMCD signal recorded at 6.5 K at a 15° grazing angle of incidence is 0.3% at the pre-edge feature for the 5% and 10% samples and 0.2% for the 15% sample. The inset shows the associated $M(H)$ curves recorded at the pre-edge feature.

A. Synchrotron measurements

Figure 1(a) shows three XANES spectra for 5%, 10%, and 15% Co-doped ZnO films fabricated by RMS together with the associated XLD. The inset enlarges the pre-edge feature of the Co K-edge stemming from $1s \rightarrow 3d,4p$ transitions, which are characteristic of Co^{2+} in tetrahedral coordination.[7–9] No difference in the pre-edge feature is visible for the three concentrations and the size of this feature is identical to that of the sample studied in Ref. 8. This result demonstrates the absence of a detectable fraction of elemental Co^0 in these samples. The size of the XLD signal, which can be used to quantify the fraction of Co dopant atoms

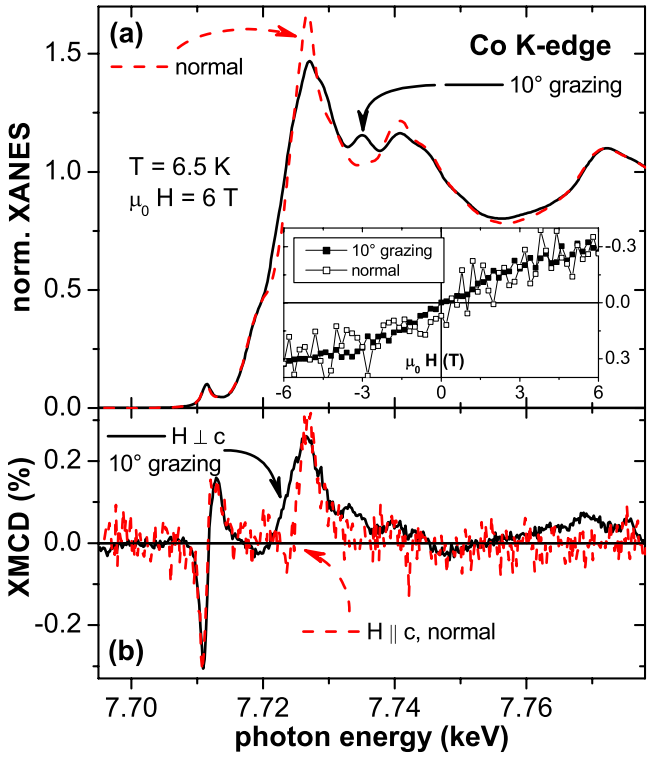

FIG. 2. (Color online) XANES and XMCD spectra recorded at the Co K edge for a PLD-grown Co:ZnO sample at 6.5 K with normal (dashed line) and 10° grazing (full line) incidence. The maximum size of the XMCD signal at the pre-edge feature is 0.3% for both orientations. The inset shows the two respective hysteresis loops recorded at the Co pre-edge feature.

located on Zn lattice sites, is of comparable size and shape to that for the sample in Ref. 8 demonstrating a very high extent of incorporation of Co dopants into the ZnO lattice. Therefore, these samples are devoid of any measurable secondary phases, in particular, elemental Co^0 so that the intrinsic properties of the Co:ZnO system can be studied. Figure 1(b) shows the respective XMCD spectra recorded at 6.5 K, 6 T, and a 15° grazing angle of incidence. Again, the spectral shape of the XMCD is indicative of Co^{2+} in tetrahedral coordination and there is no measurable elemental Co^0 (i.e., no spectral weight between the pre-edge feature and the main signal), cf. Refs. 8, 9, 16, and 17. The field dependence of the XMCD signal at the pre-edge feature was recorded at 6.5 K as well and is shown in the inset. The loop reveals paramagnetic behavior within the Co sublattice for all Co concentrations. The only obvious difference between the three XMCD spectra is the reduced size of the 15% Co:ZnO sample compared to 5% and 10%. This is a consequence of the increased probability to find Co-O-Co and higher order configurations which couple antiferromagnetically and thus do not contribute to the magnetic signal.[8,10] The reduction in the XMCD for the 15% sample will be discussed below in more detail.

Figure 2 shows the XANES and XMCD spectra recorded at 6.5 K and 6 T for the PLD-grown 10% Co-doped ZnO sample, which was previously studied in Ref. 8. In Fig. 2(a) the XANES at the Co K edge for normal and grazing incidence are shown, respectively. The difference in the spectra originates from the fact that the E vector of the circular polarized light at normal incidence rotates within the a/b plane of ZnO, whereas the E vector rotates in the a/c plane at grazing incidence. Therefore, only at grazing incidence is the true isotropic XANES probed, whereas the spectrum for normal incidence resembles the one recorded with linear polarized light with the E vector parallel to the a axis. The difference of the two XANES spectra is thus indicative of the presence of a substantial XLD effect in this sample. In Fig. 2(b) the XMCD spectra for both orientations are shown. Note that XMCD at the Co K edge is a measure of only the $4p$ orbital contribution to the total magnetic moment. This contribution is found to be isotropic and the associated $M(H)$ curves shown in the inset of Fig. 2(a) reveal that within the noise level, the two $M(H)$ curves at the Co pre-edge feature are identical and indicative of paramagnetism. This result implies a nearly isotropic orbital contribution to the total magnetization and thus a negligible difference between $g_{\parallel}$ and $g_{\perp}$ within the detection limit of K-edge XMCD (~5%).

B. Integral SQUID measurements

Figure 3 summarizes $M(H)$ curves measured by integral SQUID magnetometry for three different samples with 10% Co, two grown by RMS and one grown by PLD. For each sample, H was applied parallel and perpendicular to the c axis of the ZnO. To reliably extract the diamagnetic background, we have measured $M(H)$ curves at various temperatures from 2 to 300 K for both orientations on the same piece of sample. For all temperatures a common diamagnetic background was subtracted from the raw data, leading to a convergence to uniform $M(H)$ behavior at 300 K for all Co concentrations. Note that this background is approximately 3% different for the two different orientations of the sample because of the different filling factor of the magnetometer, as discussed in more detail in Ref. 15. Since the literature value of the zero-field splitting for Co^{2+} in ZnO is known to be $D=0.342$ meV,[1,2,13] corresponding to ~4 K thermal energy, it is reasonable to expect a vanishing anisotropy at more elevated temperatures. The isotropic behavior of the $M(H)$ curves at and above 30 K confirms the validity of this approach to determine the diamagnetic contribution from the substrate.[18] We want to stress the reproducibility of the anisotropic $M(H)$ curves for three different samples from two different laboratories as seen in Fig. 3, thereby ruling out reproducibility issues, which were already pointed out in the first report of "ferromagnetic" ZnO.[19] Note that the residual magnetic signal at 300 K on the order of <0.5 μ emu is not indicative of ferromagnetism for any of the samples.[15] For better comparability the data shown in Fig. 3 have been normalized to the magnetization measured with $H \perp c$ at 2 K and 4.5 T, which will be termed M_{sat} in the following.

C. Electron paramagnetic resonance

Figure 4 compares two EPR measurements recorded at 5 K as a function of the polar angle Θ for two different types of samples. The color-coded diagram represents the findings for a ~1-μm-thick 5% Co-doped ZnO film grown by RMS.

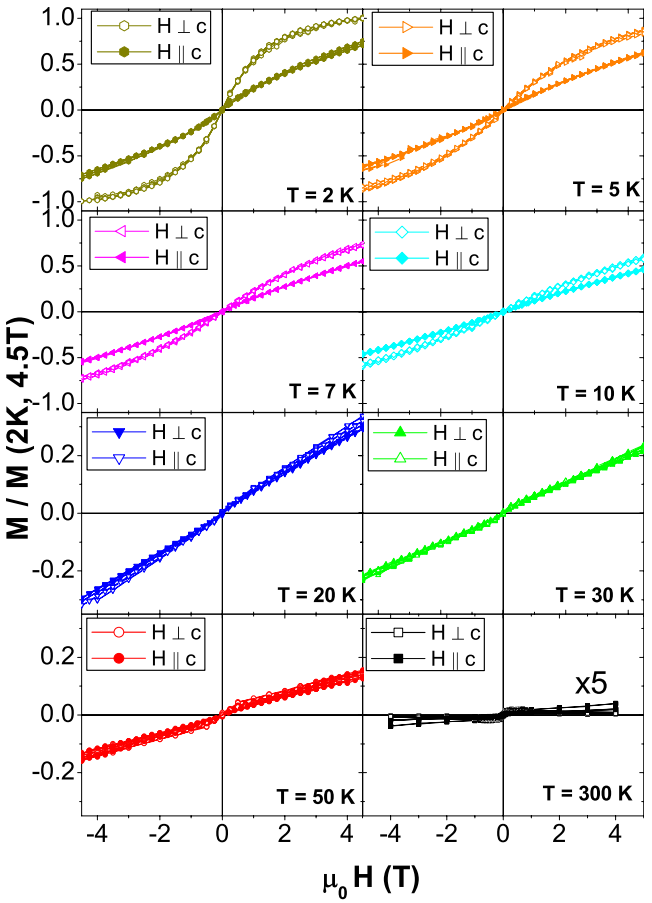

FIG. 3. (Color online) $M(H)$ curves for two RMS-grown and one PLD-grown Co:ZnO films with 10 at. % Co for $H \| c$ (open symbols) and $H \perp c$ (full symbols) at various temperatures, as measured by SQUID. All measurements have been normalized to M_{sat}, i.e., the maximum magnetization measured at 2 K, 4.5 T, and with $H \perp c$. The anisotropy increases with decreasing temperature below 30 K.

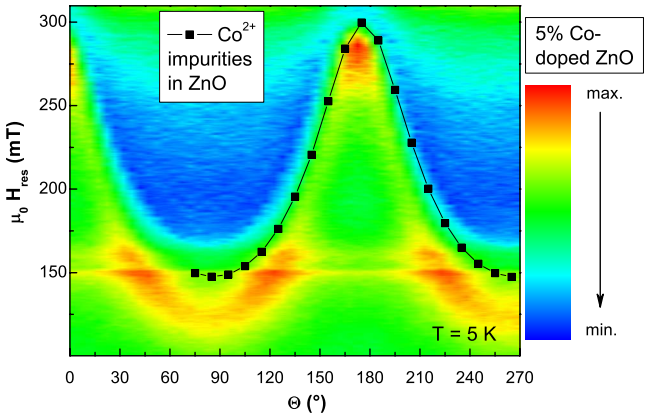

FIG. 4. (Color online) EPR color-code plot recorded at 5 K of a 5% Co-doped ZnO sample grown by RMS as a function of the polar angle Θ. A broad resonance feature with uniaxial behavior is visible. For comparison an identical EPR experiment is shown for Co^{2+} impurities in bulk ZnO (black squares).

A broad (~100 mT) resonance with uniaxial behavior is visible, which quickly vanishes upon increasing temperature. Note that the same resonance could be detected for thinner Co:ZnO samples with 5% and 10% Co. However, due to the reduced number of Co atoms and the increased broadening at 10%, the signal was much less pronounced. For comparison, a commercially available ZnO c plane substrate (CrysTec GmbH) was measured under identical conditions. This substrate contains various types of paramagnetic impurities, among them Co^{2+}, confirmed by the presence of an hyperfine-split octet (not shown). This anisotropic hyperfine splitting serves to unambiguously identify Co^{2+} (nuclear spin $I=7/2$), see Ref. 20. The center of gravity of this octet is shown as black squares in Fig. 4. The good agreement between the two experiments indicates that the g factors ($g_{\|}$ and $g_{\perp,\mathrm{eff}}$) used to model the anisotropic paramagnetic behavior do not significantly change as a function of Co concentration, independent of whether the Co is present at the impurity level or at concentrations as high as 5%. On the other hand, the hyperfine splitting is not visible for the 5% sample and the resonance line is strongly broadened, presumably due to weak dipolar interactions. Such a broadening has already been reported.[21] However, we do not find any evidence for exchange pairs. Note that the value of $g_{\perp,\mathrm{eff}}$ only weakly depends on the magnitude of D as already pointed out in Ref. 13.

D. Effective spin model

It is well established that the magnetic properties of Co^{2+} ($3d^7$) impurities in ZnO can be described by an effective $S=3/2$ spin Hamiltonian,[1,2,13]

$$\hat{H}_{spin} = \mu_B g_{\|} H_z S_z + \mu_B g_{\perp} (H_x S_x + H_y S_y) + D S_z^2, \qquad (1)$$

where the magnetic state is characterized by the two g factors $g_{\|}=2.238$ ($H \| c$) and $g_{\perp}=2.276$ ($H \perp c$) and the zero-field splitting constant D which originates from the SO interaction. The respective $^4A_2$ ground state is SO split by $2D=0.684$ meV forming two levels, $E_{1/2}$ and $E_{3/2}$ (nomenclature of Ref. 2) as measured by EPR (Ref. 1) and optical measurements on ZnO single crystals with Co impurities (10 ppm) (Ref. 2) and recently confirmed for epitaxial Co:ZnO samples.[13] The measured $M(H)$ curves for $H \| c$ for Co:ZnO samples with less than 1% of Co could be modeled with reasonable accuracy[13] using the above effective spin model. Note that also the resonance field measured by EPR could be modeled with the same g factors[13] and using $g_{\perp,\mathrm{eff}} = 2g_{\perp}[1-(3/64)(h\nu/D)^2]$ which can be approximated with $g_{\perp,\mathrm{eff}} \sim 2g_{\perp}$ for $D \gg h\nu$.[22] The weak dependence of $g_{\perp,\mathrm{eff}}$ on D is the reason why high-field EPR (~30 T) has to be used to directly determine D from resonance measurements as done in Ref. 13.

Equation (1) can be used to calculate the energy levels of the $S=3/2$ manifold $|M_s\rangle = |-3/2\rangle \cdots |3/2\rangle$ by the matrix $\langle M_s | \hat{H}_{spin} | M_s \rangle$ for $H \| c$ ($H=H_z$) and $H \perp c$ ($H=H_x$), respectively.

For $H \| c$ the matrix is diagonal and the energy levels are given by

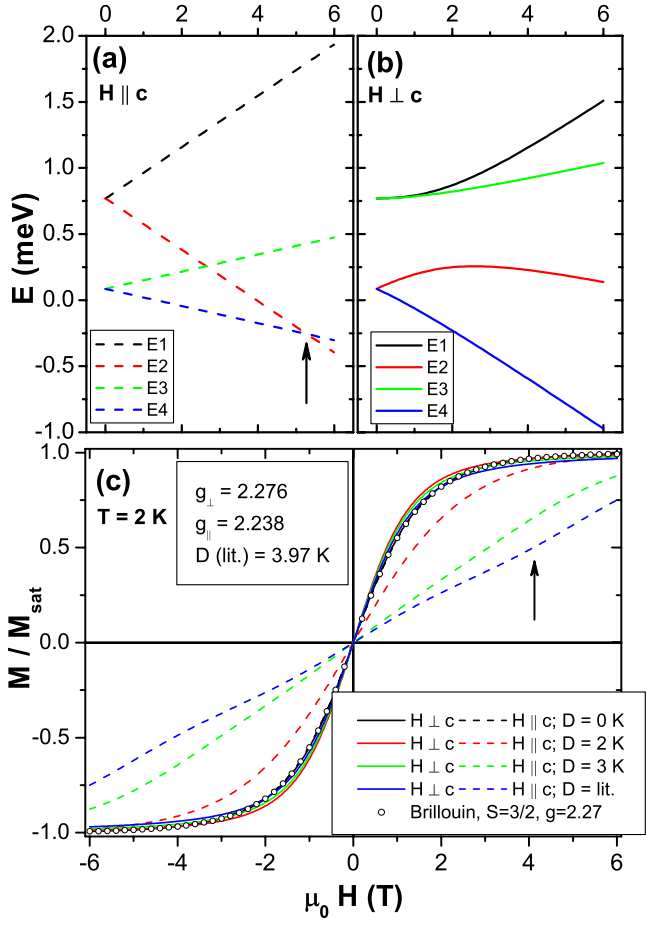

FIG. 5. (Color online) Calculated energy levels according to the effective spin model for (a) $H\|c$ and (b) $H\perp c$ using literature values. The arrow indicates the level crossing. (c) Calculated $M(H)$ curves at 2 K for $H\|c$ (dashed lines) and $H\perp c$ (solid lines) using the effective spin model and different values of the zero-field splitting D. The Brillouin function is given for comparison (open circles).

$$E_1 = \frac{9D}{4} + \frac{3}{2}\mu_B g_\| H_z \quad E_2 = \frac{9D}{4} - \frac{3}{2}\mu_B g_\| H_z,$$

$$E_3 = \frac{D}{4} + \frac{1}{2}\mu_B g_\| H_z \quad E_4 = \frac{D}{4} - \frac{1}{2}\mu_B g_\| H_z.$$

The four energy levels are plotted in Fig. 5(a) using the literature values for $g_\|=2.238$, $g_\perp=2.276$, and $D=0.342$ meV (=3.97 K). At moderate magnetic fields the lowest energy level E_4 is $S=1/2$ like. At high magnetic fields the $S=3/2$-like E_2 level becomes lower in energy indicated by an arrow in Fig. 5(a).

For $H\perp c$ the analytical diagonalization yields

$$E_1 = \frac{1}{2}\mu_B g_\perp H_x + \frac{5}{4}D + \sqrt{\mu_B^2 g_\perp^2 H_x^2 - D g_\perp \mu_B H_x + D^2},$$

$$E_2 = \frac{1}{2}\mu_B g_\perp H_x + \frac{5}{4}D - \sqrt{\mu_B^2 g_\perp^2 H_x^2 - D g_\perp \mu_B H_x + D^2},$$

$$E_3 = -\frac{1}{2}\mu_B g_\perp H_x + \frac{5}{4}D + \sqrt{\mu_B^2 g_\perp^2 H_x^2 + D g_\perp \mu_B H_x + D^2},$$

$$E_4 = -\frac{1}{2}\mu_B g_\perp H_x + \frac{5}{4}D - \sqrt{\mu_B^2 g_\perp^2 H_x^2 + D g_\perp \mu_B H_x + D^2}.$$

The resulting energy levels are plotted in Fig. 5(b). In this case the lowest energy level E_4 is $S=3/2$ like and no crossing of the energy levels occurs. It was already demonstrated that at Co concentrations above 1% the experimental $M(H)$ curves can be different from the predictions of the effective spin model. Next neighbor exchange constants $J^{\text{in/out}}$ and an effective temperature $T_{\text{eff}}=T+T_0$ had to be introduced[10] to better reproduce the data. Despite this effort, the curvature of the $M(H)$ curve could not be well reproduced, especially at low magnetic fields, which was attributed to distant neighbor interactions.[10] On the other hand, these experiments were primarily focused on SQUID measurements at 2 K with $H\|c$ and the full temperature dependence of the anisotropy of the $M(H)$ curves was not studied.

Since the EPR measurements shown in Fig. 4 have revealed that $g_\perp$ and $g_\|$ do not change significantly at high Co concentrations, the following discussion shall be limited to the role of the zero-field splitting D. Figure 5(c) shows the dependence of the anisotropy of the $M(H)$ curves on the strength of the zero-field splitting D calculated for $T=2$ K. For that purpose the magnetization $M=-(\partial F/\partial H)_T$ of the magnetic free energy $F=-k_BT\ln Z$ using the partition function $Z=\Sigma_i e^{-E_i/k_BT}$ was calculated using the energy levels shown in Figs. 5(a) and 5(b) for different values of D ranging from 0 K to the literature value of 3.97 K for $H\perp c$ (solid lines) and $H\|c$ (dashed lines). For comparison, the Brillouin function B_S for $S=3/2$ and $g_\perp=2.276$ is shown as open circles. As expected, the anisotropy decreases for decreasing D. The level crossing is barely visible as an inflection point in the $M(H\|c)$ curve [arrow in Fig. 5(c)] for $D=3.97$ K. For lower D the inflection point is fully washed out for the given temperature of 2 K. In the limit of $D=0$ K the $M(H)$ curves calculated from the Brillouin function and the effective spin model are identical [except for the tiny anisotropy stemming from the anisotropic g factor, which is barely visible in Fig. 5(c)]. On the other hand, the shape of the $M(H)$ curve for $H\perp c$ is hardly affected by the chosen value of D—only a slightly increased curvature is visible. This explains why fitting the $M(H)$ curves using the Brillouin function has previously been successful in cases were highly oriented Co:ZnO samples were studied with $H\perp c$ (in-plane measurements for c oriented ZnO samples).[8,23] Using $S=3/2$ and $g_\perp=2.276$, this yields an effective magnetic moment of $\mu=3.414\mu_B$/Co atom. The slightly increased curvature for finite D values compared to the Brillouin function is the reason that using the Brillouin function with $S=3/2$ and $L=1$, i.e., an effective moment of $\mu=4\mu_B$/Co atom yields a good reproduction of the experimental data in Ref. 8. We will come back to the Brillouin function further below.

The $M(H)$ curves for $H\|c$ show a decreasing slope with increasing D, thereby being solely responsible for the increase in anisotropy. For sufficiently large D at the given temperature of 2 K, the aforementioned inflection point be-

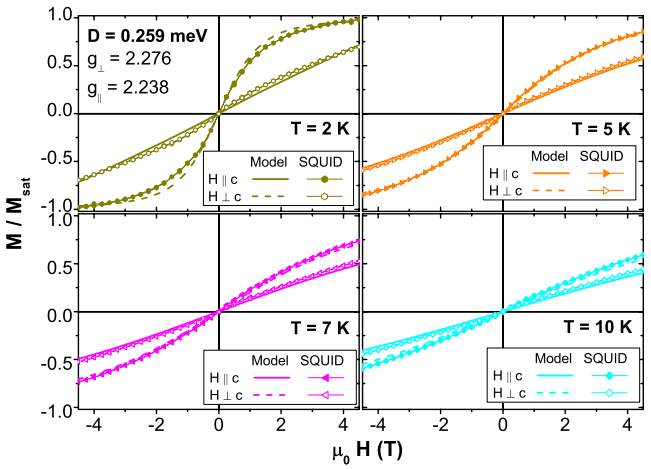

FIG. 6. (Color online) $M(H)$ curves for a 10% Co:ZnO film with $H \perp c$ (full symbols) and $H \| c$ (open symbols). Dashed and full lines are the respective $M(H)$ curves as calculated from the effective spin model. $g_\perp$ and $g_\|$ are fixed at the literate values.

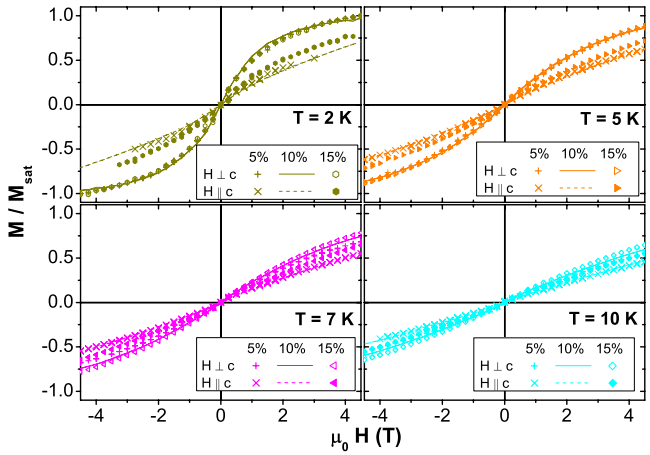

FIG. 7. (Color online) $M(H)$ curves for a 10% Co:ZnO film with $H \perp c$ (full line) and $H \| c$ (dashed line) compared to 5% (crosses) and 15% (symbols) Co:ZnO films. All data have been normalized to M_{sat}.

comes visible (marked by the arrow) which eventually evolves to the well-known magnetization step at very low temperatures. Such a step is characteristic for this type of single-ion anisotropy, see, e.g., Ref. 24. The absence of this kink in the $M(H)$ data at 2 K in Fig. 3 can be seen as a first indication that the well-established value of $D=3.97$ K may actually be lower for Co:ZnO samples with high Co concentration.

E. Modeling the anisotropic $M(H)$ curves

Figure 6 compiles a selection of experimental $M(H)$ curves with the calculation using the effective spin model. The experimental data for $H \perp c$ (full symbols) and $H \| c$ (open symbols) have been normalized to M_{sat} as in Fig. 3. Therefore, these data are representative of all three 10% Co:ZnO samples. Since the EPR measurements have not revealed any indication for an altered g factor (see Fig. 4), only the zero-field splitting D is used as free fitting parameter. The best agreement is yielded using $D=0.259$ meV corresponding to 3.01 K. Obviously, the experimental data suggest that the zero-field splitting D is reduced to ~ 3 K instead of the well-established literature value of ~ 4 K. On the other hand, D was determined from bulk ZnO crystals with Co impurities in Refs. 1 and 2 and for 1–2 % Co-doped single crystals at high magnetic fields between 10 and 30 T.[13] Therefore, the value for D in 10% Co:ZnO epitaxial films is not available in the literature. Note that the anisotropy of the $M(H)$ curves measured by SQUID was only reported for a 0.28% Co:ZnO film at 2 K in Ref. 13.

F. Co concentration dependence

Figure 7 shows the anisotropic $M(H)$ curves for Co concentrations of 5%, 10%, and 15% normalized to M_{sat}. At 2 and 5 K the $M(H \perp c)$ curves coincide for 5% (+), 10% (full line), and 15% (open symbol). In contrast, for the $M(H \| c)$ curves only the 5% ($\times$) and 10% (dashed line) data coincide, whereas the 15% sample (full symbols) exhibits systematically higher magnetization values, i.e., a reduced anisotropy. The situation is more complex at 7 and 10 K. As with 2 and 5 K, the 5% and 10% samples show identical $M(H \| c)$ behavior and the 15% sample has a systematically higher magnetization. On the other hand, the $M(H \perp c)$ curves start to differ in that the 15% sample has a higher magnetization than the 10% sample, whereas the 5% sample has a reduced magnetization. This trend (not shown) continues at more elevated temperatures but is less pronounced. In general, the $M(H)$ curves for the 15% sample show the slowest reduction with temperature and the 5% the strongest. The anisotropy is virtually identical for the 5% and the 10% samples and well described by $D=3$ K, whereas the anisotropy is reduced for the 15% sample to below 2 K. Finally, at 300 K, none of the three samples show any significant magnetization beyond the detection limit of the SQUID as expected for paramagnetic samples.

G. Modeling using the Brillouin function

Figure 8 shows the experimental data shown in Fig. 3 together with the calculated magnetization curves from Fig. 5 (i.e., effective spin model with $D=3.97$ K) for $H \perp c$ and $H \| c$ now plotted versus H/T. First, we will focus on the first and third columns, where the nominal experimental temperature has been used to derive H/T. Whereas the $M(H/T)$ curves coincide at all temperatures for $H \perp c$, the behavior for $H \| c$ indicates a temperature-driven cross over from the $E_{1/2}$ to the $E_{3/2}$ state. As columns two and four in Fig. 8 demonstrate, the introduction of an effective temperature $T_{\text{eff}}=T+T_0$ leads to coinciding $M(H/T)$ curves for $H \| c$ as well. Note that also for $H \perp c$, a small T_0 of 0.5 K has to be introduced for $T=2$ K. The respective values for T_0 given in the legend of Fig. 8 are identical for the experimental data and the calculation based on the effective spin model. Therefore, the anisotropy and temperature dependence of the $M(H)$ curves as described by the effective spin model and measured by SQUID can be qualitatively modeled by a Brillouin-type paramagnet together with a simple effective

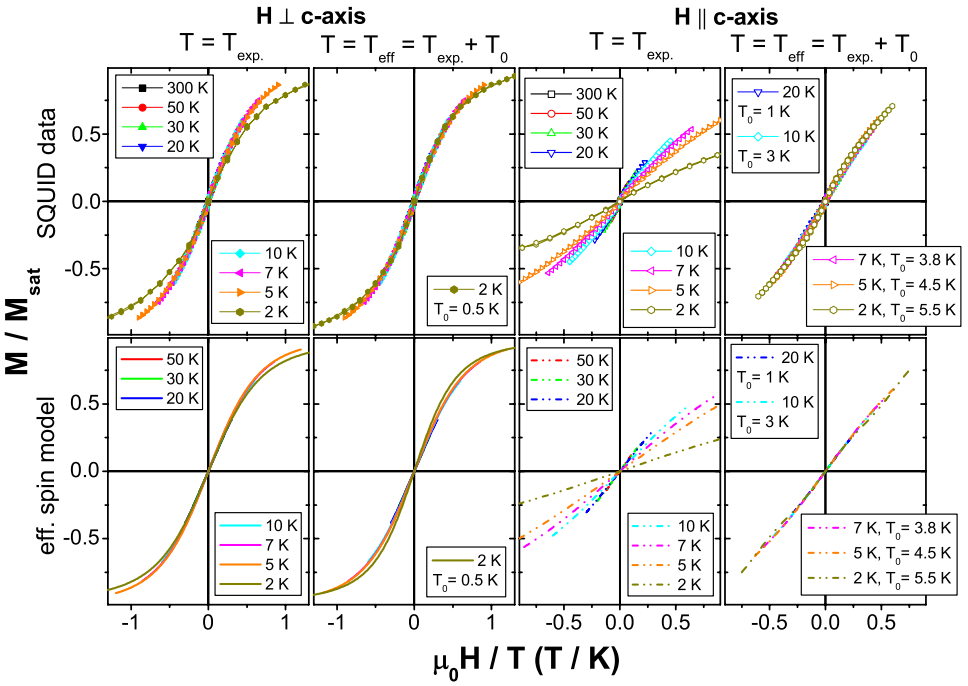

FIG. 8. (Color online) $M(H/T)$ curves for 10% Co:ZnO (top row) and for the effective spin model with $D=3.97$ K (bottom row) for $H\perp c$ (left) and $H\|c$ (right) from 2 K to 300 K. The curves are plotted either versus the nominal temperature T (first and third columns) or versus an effective temperature $T_{\text{eff}}=T+T_0$ (second and fourth columns). The value of T_0 is given in the respective legends.

temperature ansatz without explicitly taking into account the underlying microscopic origin of the anisotropy described by D in the effective spin model. Note that usually the modeling is done with T_0 being temperature independent in cases where an exchange interaction is modeled in the limit of $k_BT \gg \mu\mu_0H$ using a modified Curie-Weiss law $\chi=C/T_{\text{eff}}$. In the case of the paramagnetic single ion anisotropy studied here, where $k_BT\sim\mu\mu_0H\sim D$, T_0 has to be temperature dependent to fully account for the temperature-dependent magnetic properties. Therefore, it is important to derive T_0 directly from the effective spin model (and not from the experimental data) before additional interactions such as distant neighbor interactions beyond the single ion anisotropy can be inferred from a T_{eff} ansatz.

In Fig. 9 the same experimental data are shown as in Fig. 6. In this case, the respective modeling is done using the Brillouin function B_J for the total magnetic moment $J=S=3/2$ and $g=g_\perp=2.276$. Furthermore, we take T_{eff} as determined by the coinciding $M(H/T)$ curves from Fig. 8 to calculate the $M(H\|c)$ curves. This simple model reproduces the measured SQUID data surprisingly well. On the other hand, T_0 depends on D if T_0 is extracted from the procedure illustrated in Fig. 8. Thus, the magnitude and temperature dependence of T_0 can only provide an order-of-magnitude estimate for the effective anisotropy and is not suitable to directly determine D. Nevertheless, Fig. 9 illustrates well that Co^{2+} in ZnO can also be approximated by an ideal Brillouin paramagnet with $S=3/2$, an admixture of an orbital contribution as reflected by $g=2.276$, i.e., $L\sim 0.14$, and a weak single ion anisotropy heuristically captured by T_0. Especially for $H\perp c$ the influence of the single ion anisotropy on the shape of the $M(H)$ curves is very weak, *cf.* Fig. 5(c).

IV. DISCUSSION AND CONCLUSION

The comprehensive angular and temperature-dependent magnetic characterization of Co:ZnO epitaxial films with Co concentrations of 5%, 10%, and 15% allows us to study the intrinsic properties of Co:ZnO at high concentrations. Recording the angular and temperature dependence of the $M(H)$ curves by SQUID allows us to properly remove the diamagnetic background from the substrate. The entire set of temperature- and angular-dependent $M(H)$ curves can be

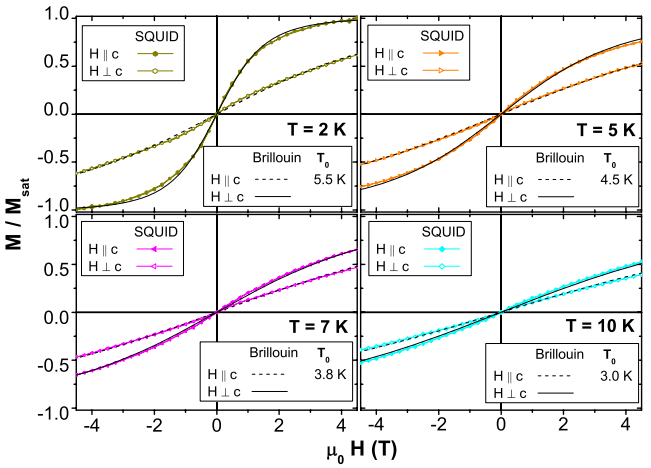

FIG. 9. (Color online) $M(H)$ curves for a 10% Co:ZnO film with $H\perp c$ (full symbols) and $H\|c$ (open symbols). Dashed and full lines are the $M(H)$ curves as calculated from the Brillouin function with $T_{\text{eff}}=T+T_0$ and T_0 as determined from Fig. 8 for $H\|c$.

TABLE I. Relative probability and absolute concentration of singles and open triples of Co in wurtzite ZnO.

Co concentration (%)	Single probability (%)	Single concentration (%)	Triple probability (%)	Triple concentration (%)
5	54.0	2.70	9.3	0.47
10	28.2	2.82	10.4	1.04
15	14.2	2.13	6.0	0.90

described well by the effective spin model using $S=3/2$, $g_{\perp}=2.276$, $g_{\parallel}=2.238$ and a positive zero-field splitting D.[1,2,13] However, the literature value of $D=0.342$ meV corresponding to 3.97 K must be reduced to $D=3$ K for the 5% and 10% Co:ZnO samples, and even further to $D\sim 2$ K for the 15% sample in order to achieve good agreement.

The experimental evidence that D is reduced to about 75% of the well-established literature value is worthy of brief discussion. According to recent work based on crystal field theory, D can be calculated from the spin-orbit interaction λ, the cubic crystal field splitting Δ, the Racah parameter B, and the trigonal parameters ν and ν',[13,25]

$$D=\frac{\lambda^2}{\Delta}\left[2\frac{\nu}{\Delta}-\frac{10\sqrt{2}}{3}\frac{\nu'}{\Delta}\left(1+\frac{4}{75}\frac{\Delta}{B}\right)\right]. \quad (2)$$

There is no obvious reason to alter λ and the cubic parameter Δ so that the most plausible explanation of a reduction in D would be a reduction in one or both trigonal parameters ν and ν'. These parameters are directly correlated with the positions of the O^2—ions surrounding the Co^{2+} ions.[25] The epitaxial growth of ZnO on a sapphire substrate can significantly alter the strain state of the film and, thus, the lattice parameters. In this context, we note that the c lattice parameter as probed by XRD for Co:ZnO thin (on the order of 100 nm) films is usually shifted to smaller angles in conventional ω-2θ scans,[6,26] i.e., the c lattice parameter is increased compared to ZnO single crystals. Such small changes in the lattice parameter do not significantly alter the XLD signature for Co:ZnO so that a small change in lattice parameters for epitaxial Co:ZnO films is not in contradiction with the findings in Fig. 1. On the one hand, the 15% sample does not only show a decreased D compared to the 10% sample but also a ZnO(002) reflection shifted to a smaller angle of 34.08° compared to 34.21°. On the other hand, the 5% sample exhibits the same D as the 10% sample but also exhibits a shifted ZnO(002) reflection (34.12°). Thus, a direct correlation between the average c lattice parameter as measured by XRD and D cannot be inferred from the data. The Co concentration also has to be taken into account.

Over the Co concentration range of 5–15 %, the formation of Co-O-Co pairs, Co-O-Co-O-Co triples, etc., becomes increasingly important. Assuming a random substitution of Zn atoms by Co, one can use Behringer's equations[27] to calculate to probability of singles (isolated Co atoms without a second Co atom in the next-cation neighbor shell), pairs, and open and closed triples. Larger configurations are nontrivial to calculate. However, the situation becomes more simple if one takes into account that Co-O-Co pairs couple antiferromagnetically. Since in case of antiferromagetic next-neighbor interaction the vast majority of Co-O-… configurations with an even number of Co atoms are expected to exhibit a fully compensated magnetic moment, the focus of the discussion is on configurations containing odd numbers of Co. In the ideal case almost all configurations with odd numbers will have only one uncompensated Co moment. Therefore, the effective moment of the configuration and thus the contribution to the measured magnetization scales like $1/n$, with n being the (odd) number of Co atoms. Therefore, triples yield the dominant additional contribution beyond the singles to the magnetization. Table I summarizes the probability of singles and open triples according to Ref. 27 for the three relevant concentrations of Co. Closed triples, which are presumably magnetically frustrated due to the antiferromagnetic next-neighbor interaction, are much more rare than open triples (about four times less likely for 10% Co). The respective concentration of singles and triples is obtained by multiplying the probability by the Co concentration. This analysis yields virtually the same concentration (2.7–2.8 %) of singles for 5% and 10% Co, whereas it is lowered to 2.1% for 15% Co doping. The magnetic behavior as measured by XMCD, see Fig. 1, also indicates that the 5% and 10% samples have the same size dichroic signal of 0.3%, whereas the 15% sample shows a reduced dichroism of 0.2%, which is also consistent with ascribing the magnetic response predominantly to the singles.

At first sight it may appear tempting to assign the observed anisotropy exclusively to the Co singles, by assuming isotropic behavior to all higher odd configurations. The most extreme case, i.e., Co singles having the full zero-field splitting $D=3.97$ K and the triples having $D=0$ K [i.e., isotropic, Brillouin-type $M(H)$ curves], one can model the resulting $M(H\|c)$ curves by adjusting the sum of the two contributions to the $M(H\perp c)$ curve. However, even is this most extreme case, the expected anisotropy is still larger than the observed value (not shown). Therefore, we have to conclude that Co singles also have a reduced D compared to Co^{2+} impurities. Providing concrete values of D for singles and triples is however not possible in a meaningful manner since the mathematical problem is under determined.

On the other hand, the probabilities shown in Table I can be used to explain the different temperature dependencies of the $M(H)$ curves for the three Co concentrations at 7 and 10 K in Fig. 7. Let us first consider the 15% sample. The concentration of singles (2.13%), pairs (1.45%), and open triples (0.90%) accounts only for less than 1/3 of all Co ions present in this sample. That means that more than 2/3 of all Co atoms are present as larger Co-O… configurations, which are

likely to be in a magnetically frustrated state, in particular, the configurations containing odd numbers of Co. It is therefore plausible to assume that at higher temperatures, such frustrated configurations can follow the external field more easily leading to an increasing contribution to the magnetization beyond the expectations of the effective spin model. In turn, the 5% sample has fewer of these higher configurations since singles (2.70%), pairs (1.19%), and open triples 0.47% constitute already about 87% of all Co ion present in this sample so that only a fraction of about 13% of all Co atoms are present in larger configurations. Consequently, virtually no additional magnetization beyond the expectations of the effective spin model appears at more elevated temperatures leading to a more pronounced decrease in the magnetization with temperature. Comparing the $M(H)$ curves at 10 K in Fig. 6 (10% sample versus effective spin model) and in Fig. 7 (5% versus 10%), one recognizes that the 5% sample indeed follows the expectation of the effective spin model quite well, underlining that the magnetic behavior of the 5% sample is well described by Co singles having a reduced D and aniferromagnetically coupled Co-O-Co pairs.

Whether the reduction in D of the 5% sample can be assigned to distant neighbor interactions or to distortions of the lattice of the epitaxial film cannot ultimately be answered since no ZnO singles crystals with a Co concentration of 5% have been studied yet. The only available experiment directly determining D was done for 1–2 % of Co in a ZnO single crystal by high-field EPR.[13] If one considers this as reference for an undistorted ZnO doped with a comparable amount of Co, the reduction in D for 5% Co:ZnO epitaxial films originates from the distortion of the lattice as reflected by the shifted ZnO(002) reflection as measured with XRD. In turn this would imply negligible magnetic interactions beyond next-neighbor antiferromagnetic coupling. However, negligible magnetic interactions at these Co concentrations would be in contradiction with the findings in Ref. 10, where an effective temperature had to be introduced to properly model the $M(H\|c)$ curves for Co concentrations of 3.4% and 5.2% [in thick ($\sim$1 μm) epitaxial films]. On the other hand, the anisotropy of the samples in Ref. 10, i.e., the difference between $M(H\|c)$ and $M(H\perp c)$ has not been studied as a function of Co concentration. In this context it should be noted that the relative insensitivity of the $M(H\perp c)$ curve to the chosen value of D as shown in Fig. 5(c) can serve as a viable way to properly normalize different experiments, in order to reliably study a dependence of D on the Co concentration. Only in this case, the distant neighbor interactions can be probed in a meaningful manner by $M(H)$ curves.

Finally, the assumption of an antiferromagnetic next-cation neighbor interaction has to be briefly discussed. It has previously been invoked experimentally for bulk Co:ZnO (Refs. 3 and 4) and epitaxial films.[8,10] The former used a Curie-Weiss analysis with negative Curie-Weiss temperatures Θ of the order of 100 K. The latter has been demonstrated via a reduction in the measured magnetization compared to the expected magnetization inferred from the number of Co atoms and the Co magnetic moment. Note that a direct determination of the magnitude of the antiferromagnetic interaction is not possible from this procedure; however, a Curie-Weiss analysis of the inverse susceptibility as a function of temperature clearly shows net-antiferromagnetic interactions with a negative Curie-Weiss temperature Θ of about 150 K for the present samples (not shown) which compares well with previous findings.[3] An antiferromagnetic alignment of Co-O-Co configurations is also supported by theory. An antiferromagnetic Co-O-Co interaction on the order of 10–20 K was already discussed combining experiment and theory, see Ref. 10 and references therein. More recent *ab initio* calculations provide evidence of an even stronger Co-O-Co interaction on the order of 10 meV, however, with competing ferro- and antiferromagnetic alignment parallel and perpendicular to the c axis.[12] The antiferromagnetic interaction is also consistent with the antiferromagnetic exchange interaction of −36.7 meV calculated for CoO in wurtzite structure.[28] It is therefore plausible to assume magnetically compensated Co-O-Co configurations at least in the temperature range from 2 to 15 K discussed here both from previous experimental and theoretical findings indicating a fairly strong antiferromagnetic interaction.

In summary, we have studied the angular- and temperature-dependent magnetic properties of Co:ZnO for three different Co concentrations—5%, 10%, and 15%. Element specific as well as integral magnetometry reveal only paramagnetism. The high degree of structural quality has been demonstrated by means of XLD and XANES. In particular, these measurements provide strong evidence for virtually all Co being in the +2 formal charge state and at Zn sites in the lattice. XMCD and EPR measurements indicate a very small anisotropy for the orbital contribution to the magnetic moment being consistent with the well-established values of $g_{\perp}=2.276$ and $g_{\|}=2.238$ for Co^{2+} impurities in bulk ZnO. Detailed SQUID measurements reveal a paramagnetic anisotropy which is well described by the common effective spin model with a positive zero-field splitting D. However, D is found to be reduced to 3 K (75% of the value for Co^{2+} impurities) for 5% and 10% Co and even further to $\sim$2 K for 15% Co. This reduction is most likely caused by lattice distortions present in these epitaxial films. However, the increased reduction for the 15% sample must comprise other mechanisms such a lower effective anisotropy of larger Co-O-… configurations. Deviations from the magnetic behavior at more elevated temperatures can be explained by contributions of large Co-O-… configurations which increase with increasing Co concentration. In all experiments, no distant neighbor magnetic interactions could be unambiguously detected beyond the dipolar line broadening observed in EPR and no indications of ferromagnetism have been found. This conclusion is corroborated by the applicability of the effective spin model developed for noninteracting Co^{2+} impurities at the parts per million level to Co:ZnO epitaxial films with Co concentration as high as 15%.

ACKNOWLEDGMENTS

This work was supported by the EU under Grant No. MEXT-CT-2004-014195. A portion of the research was performed using EMSL, a national scientific user facility sponsored by the Department of Energy, Office of Biological and

Environmental Research located at Pacific Northwest National Laboratory. The PNNL work was supported by the U.S. Department of Energy, Office of Science, Office of Basic Energy Sciences, Division of Materials Science and Engineering Physics. Many helpful discussions with K. Usadel are gratefully acknowledged, especially regarding the diagonalization of the effective spin model and for critically reading the manuscript.

*ney@maglomat.de

[1] T. L. Estle and M. de Wit, Bull. Am. Phys. Soc. **6**, 445 (1961).
[2] P. Koidl, Phys. Rev. B **15**, 2493 (1977).
[3] S. Kolesnik, B. Dabrowski, and J. Mais, J. Appl. Phys. **95**, 2582 (2004).
[4] G. Lawes, A. S. Risbud, A. P. Ramirez, and R. Seshadri, Phys. Rev. B **71**, 045201 (2005).
[5] T. C. Kaspar, T. Droubay, S. M. Heald, P. Nachimuthu, C. M. Wang, V. Shutthanandan, C. A. Johnson, D. R. Gamelin, and S. A. Chambers, New J. Phys. **10**, 055010 (2008).
[6] M. Opel, K.-W. Nielsen, S. Bauer, S. T. B. Goennenwein, J. C. Cezar, D. Schmeisser, J. Simon, W. Mader, and R. Gross, Eur. Phys. J. B **63**, 437 (2008).
[7] T. C. Kaspar, T. Droubay, S. M. Heald, M. H. Engelhard, P. Nachimuthu, S. A. Chambers, Phys. Rev. B **77**, 201303(R) (2008).
[8] A. Ney, K. Ollefs, S. Ye, T. Kammermeier, V. Ney, T. C. Kaspar, S. A. Chambers, F. Wilhelm, and A. Rogalev, Phys. Rev. Lett. **100**, 157201 (2008).
[9] A. Ney, M. Opel, T. C. Kaspar, V. Ney, S. Ye, K. Ollefs, T. Kammermeier, S. Bauer, K.-W. Nielsen, S. T. B. Goennenwein, M. H. Engelhard, S. Zhou, K. Potzger, J. Simon, W. Mader, S. M. Heald, J. C. Cezar, F. Wilhelm, A. Rogalev, R. Gross, and S. A. Chambers, New J. Phys. **12**, 013020 (2010).
[10] P. Sati, C. Deparis, C. Morhain, S. Schäfer, and A. Stepanov, Phys. Rev. Lett. **98**, 137204 (2007).
[11] S. K. Nayak, M. Ogura, A. Hucht, S. Buschmann, H. Akai, and P. Entel, Phys. Status Solidi A **205**, 1839 (2008).
[12] S. K. Nayak, M. Ogura, A. Hucht, H. Akai, and P. Entel, J. Phys.: Condens. Matter **21**, 064238 (2009).
[13] P. Sati, R. Hayn, R. Kuzian, S. Régnier, S. Schäfer, A. Stepanov, C. Morhain, C. Deparis, M. Laügt, M. Goiran, and Z. Golacki, Phys. Rev. Lett. **96**, 017203 (2006).
[14] A. Rogalev, J. Goulon, C. Goulon-Ginet, and C. Malgrange, Lect. Notes Phys. **565**, 61 (2001).
[15] A. Ney, T. Kammermeier, V. Ney, K. Ollefs, and S. Ye, J. Magn. Magn. Mater. **320**, 3341 (2008).
[16] K. Rode, R. Mattana, A. Anane, V. Cros, E. Jacquet, J.-P. Contour, F. Petroff, A. Fert, M.-A. Arrio, Ph. Sainctavit, P. Bencok, F. Wilhelm, N. B. Brookes, and A. Rogalev, Appl. Phys. Lett. **92**, 012509 (2008).
[17] T. Büsgen, M. Hilgendorff, S. Irsen, F. Wilhelm, A. Rogalev, D. Goll, and M. Giersing, J. Phys. Chem. C **112**, 2412 (2008).
[18] It is critical to note that the diamagnetic background for $H \| c$ is larger, i.e., if one takes the diamagnetism as isotropic and determines it from the $H \perp c$ data, the slope of the resulting $M(H \| c)$ curve will be reduced so that the anisotropy appears to be larger.
[19] K. Ueda, H. Tabata, and T. Kawai, Appl. Phys. Lett. **79**, 988 (2001).
[20] N. Jedrecy, H. J. von Bardeleben, Y. Zheng, and J.-L. Cantin, Phys. Rev. B **69**, 041308(R) (2004).
[21] P. Sati, A. Stepanov, and V. Pashchenko, Low Temp. Phys. **33**, 927 (2007).
[22] W. C. Holton, J. Schneider, and T. L. Estle, Phys. Rev. **133**, A1638 (1964).
[23] A. Barla, G. Schmerber, E. Beaurepaire, A. Dinia, H. Bieber, S. Colis, F. Scheurer, J.-P. Kappler, P. Imperia, F. Nolting, F. Wilhelm, A. Rogalev, D. Müller, and J. J. Grob, Phys. Rev. B **76**, 125201 (2007).
[24] Y. Shapira and V. Bindilatti, J. Appl. Phys. **92**, 4155 (2002).
[25] R. O. Kuzian, A. M. Daré, P. Sati, and R. Hayn, Phys. Rev. B **74**, 155201 (2006).
[26] T. Kammermeier, V. Ney, S. Ye, K. Ollefs, T. C. Kaspar, S. A. Chambers, F. Wilhelm, A. Rogalev, and A. Ney, J. Magn. Magn. Mater. **321**, 699 (2009).
[27] R. E. Behringer, J. Chem. Phys. **29**, 537 (1958).
[28] Th. Archer, R. Hanafin, and S. Sanvito, Phys. Rev. B **78**, 014431 (2008).